

Modelling of Large Tilting Pad Thrust Bearing Stiffness and Damping Coefficients

Tilting pad thrust bearings are designed to transfer high axial loads from rotating shafts with minimum power loss. In the present paper, formulation of Reynolds' equation for the bearing is done in two dimensions (planar). A finite difference method is used to convert the terms of the Reynolds' equation into a set of simultaneous linear algebraic equations. A solution procedure for finding value of the pressure in the oil film is described. Numerical integration of the pressure values gives the load distribution. Subsequently, the study of dynamic stiffness and damping characteristics of the bearing is done by varying the value of the oil film thickness and introducing vertical velocity in the runner. Large thrust bearing behavior in a realistic configuration allowing sufficient parameter variation to check the fidelity of this analytical model is to be developed. This data is useful as an input for rotor dynamics studies of the vertical rotors. The agreement supports the fidelity and accuracy of the software package and its continued use in analysis and design.

Keywords: linear stiffness, damping, planar, thrust bearing

1. INTRODUCTION

Each bearing consists of a series of pads supported in a carrier ring as shown in figure 1; each pad is free to tilt so that it creates a self-sustaining hydrodynamic film. There are two main types of dynamic condition common to all bearings as studied in [1]. One condition is concerned with dynamically loaded bearings such as in internal combustion engines in which the load is constantly changing in magnitude and direction.

The other dynamic condition is when acceleration occurs. This takes place when a sudden space change occurs in an operating turbine. A knowledge of how the oil film builds up as the rotational speed, increases is of vital importance with a view to promoting the rapid formation of a thick oil film separating the two bearing components.

To date there has been a minimal effort to evaluate the transient response of a slider bearing undergoing acceleration in the tangential direction. Unsteady operation is one of the primary mechanisms of failure in a fluid bearing.

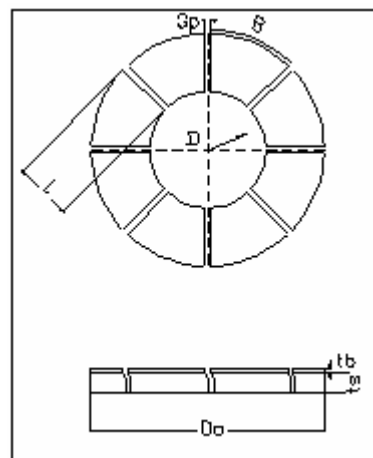


Figure 1. Geometry of the thrust pad

D.V. Srikanth¹⁾, K.K. Chaturvedi²⁾.

A. Chenna Kesava Reddy³⁾

1)Bharat Institute of Engineering and Technology
Mangalpally, Hyderabad, A.P., India

dvsrikanth1@hotmail.com

2)Bharath Heavy Electricals Limited (R&D)

Vikas Nagar, Hyderabad, A.P., India

chaturvedi@bhelrnd.co.in

3)JNTU Engineering College, Hyderabad, A.P. India

e-mail: dr_acreddy@yahoo.com

The transient response of the thrust bearing has been studied numerically as in [2] and of greatest interest is the mode of boundary layer formation and the subsequent development of the pressure in the supporting film. The supporting film is found to be fully developed in the course of a few milliseconds. The most interesting discovery was that in a tilting pad bearing the center of pressure

which corresponds to the centre of pressure which corresponds to the pivot point is a function of the film ratio.

2. REYNOLDS' EQUATION

The analysis of hydrodynamic thrust bearings have been based on Reynolds' equation for the pressure distribution. With the increasing capacity of computers numerical models including the influences of viscosity variations along and across the lubricating film have been developed. Deformation of the bearing pads due to pressure and thermal gradients were also considered.

If only the lowest order terms are retained, these can be introduced in the continuity equation which is then integrated across the fluid film to give the Reynolds' equation. The temperature of the runner along its runner surface varies much less than the temperature in the thrust pads active face. The 'flash' temperature of the runner varies by less than 1°C and the temperature along thrust pad rises by 15 to 20°C as in [3]. Values of viscosity obtained from the temperature field in the oil film are substituted in the Reynolds' equation, to determine the pressure field. In load estimation the pressure 'fitting' at the edges has been made more appropriate to suit realistic conditions as in [4].

The generalized Reynolds' equation for rectangular thrust segment is :

$$\frac{\partial}{\partial x} \left[F_2 \frac{\partial p}{\partial x} \right] + \frac{\partial}{\partial y} \left[F_2 \frac{\partial p}{\partial y} \right] = \frac{\partial}{\partial y} \left[\frac{F_3}{F_0} U \right] \quad (1)$$

$$\text{Where, } F_0 = \int_0^h \frac{d\zeta}{\mu}$$

$$F_2 = \rho \int_0^h \frac{\zeta}{\mu} (\zeta - \bar{\zeta}) d\zeta$$

$$F_3 = \rho \int_0^h (\zeta / \mu) d\zeta$$

$$\bar{\zeta} = \int_0^h (\zeta / \mu) d\zeta / \int_0^h (d\zeta / \mu)$$

F_0 , F_2 and F_3 are the viscosity integrals with units of $\text{m}^2.\text{sec}/\text{kg}$, $\text{m}.\text{sec}$ and sec respectively. Neglecting variation of viscosity across the thickness of the film, the Reynolds' equation for a sector-shaped thrust segment for incompressible lubricant, under steady state condition is derived as in

$$\frac{\partial}{\partial r} \left[\frac{rh^3}{\mu} \frac{\partial p}{\partial r} \right] + \frac{1}{r} \frac{\partial}{\partial \theta} \left[\frac{h^3}{\mu} \frac{\partial p}{\partial \theta} \right] = 6\omega r \frac{\partial h}{\partial \theta} + 12r \frac{\partial h}{\partial t} \quad (2)$$

Usual assumptions are made in the analysis done herein. The Reynolds' equation in non-dimensional form is:

$$2 \frac{\partial}{\partial R} \left[\frac{RH^3}{\bar{\mu}} \right] \frac{\partial p}{\partial R} + \frac{2RH^3}{\bar{\mu}} \frac{\partial^2 P}{\partial R^2} + \frac{2}{\beta^2 R} \frac{\partial P}{\partial \theta} \frac{\partial}{\partial \theta} \left[\frac{H^3}{\bar{\mu}} \right] \\ + \frac{2}{\beta^2 R} \frac{H^3}{\bar{\mu}} \frac{\partial^2 P}{\partial \theta^2} = 12R \frac{\partial H}{\partial \theta} + 24R \beta \frac{\partial H}{\partial t} \quad (3)$$

As compared to the above form of the equation, better numerical accuracy can be obtained, if all the first derivative terms in the equation are converted in to second derivative terms. Adopting this procedure the following equation is obtained.

$$\frac{\partial^2}{\partial R^2} \left[\frac{RH^3 p}{\bar{\mu}} \right] + \frac{RH^3}{\bar{\mu}} \frac{\partial^2 P}{\partial R^2} \\ - P \frac{\partial^2}{\partial R^2} \left[\frac{RH^3}{\bar{\mu}} \right] + \frac{1}{R\beta^2} \frac{\partial^2}{\partial \theta^2} \left[\frac{H^3 P}{\bar{\mu}} \right] \\ + \frac{1}{R\beta^2} \frac{H^3}{\bar{\mu}} \frac{\partial^2 P}{\partial \theta^2} - \frac{P}{R\beta^2} \frac{\partial^2}{\partial \theta^2} \left[\frac{H^3}{\bar{\mu}} \right] \\ = 12R \frac{\partial H}{\partial \theta} + 24R\beta V \quad (4)$$

3. COMPUTATIONAL PROCEDURE

Solution of Reynolds' equation using FDM discretization of thrust pad is done by considering a total of 81 nodes in the form of a grid as shown in figure 2. The Reynolds' equation is a non-homogeneous partial differential equation of two variables for which closed form analytical solutions are not available. The use of finite difference methods for a numerical approximation of this type of partial differential equation is discussed in [5].

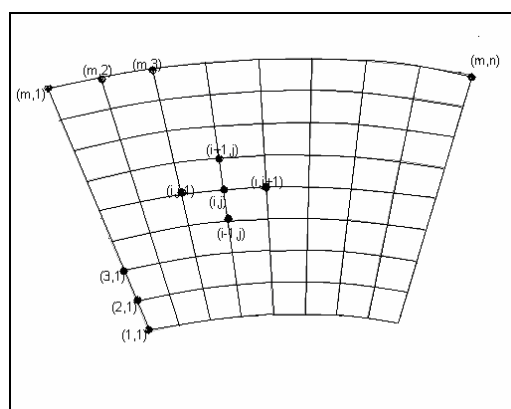


Figure 2. Discretization of pad for Reynold's equation

The finite difference equation is derived by approximating the derivatives in the differential equation via the truncated Taylor series expansion for three successive grid points. The central difference form where in the values of the function at adjacent nodes on either side are required to evaluate the derivatives is used.

Writing the Reynolds' equation in the above finite difference form as in (5) results in a set of linear algebraic equations which can be transformed into matrix form and solved simultaneously by available subroutines. This yields the non-dimensional pressure at each node.

$$\begin{aligned}
 & P_{i+1,j} \left[\frac{R_{i,j} H_{i,j}^3}{\Delta R^2 \bar{\mu}_{i,j}} + \frac{R_{i+1,j} H_{i+1,j}^3}{\bar{\mu}_{i+1,j} \Delta R^2} \right] \\
 & + P_{i-1,j} \left[\frac{R_{i,j} H_{i,j}^3}{\Delta R^2 \bar{\mu}_{i,j}} + \frac{R_{i-1,j} H_{i-1,j}^3}{\bar{\mu}_{i-1,j} \Delta R^2} \right] \\
 & + P_{i,j+1} \left[\frac{H_{i,j}^3}{R_{i,j} \bar{\mu}_{i,j} \beta^2 \Delta \bar{\theta}^2} + \frac{H_{i,j+1}^3}{R_{i,j} \bar{\mu}_{i,j+1} \beta^2 \Delta \bar{\theta}^2} \right] \\
 & + P_{i,j-1} \left[\frac{H_{i,j}^3}{R_{i,j} \bar{\mu}_{i,j} \beta^2 \Delta \bar{\theta}^2} + \frac{H_{i,j-1}^3}{R_{i,j} \bar{\mu}_{i,j-1} \beta^2 \Delta \bar{\theta}^2} \right] \\
 & + P_{i,j} \left[-2 \frac{R_{i,j}}{\Delta R^2} \frac{H_{i,j}^3}{\bar{\mu}_{i,j}} - \frac{R_{i+1,j}}{\bar{\mu}_{i+1,j}} \frac{H_{i+1,j}^3}{\Delta R^2} - \frac{R_{i-1,j}}{\bar{\mu}_{i-1,j}} \frac{H_{i-1,j}^3}{\Delta R^2} \right. \\
 & \left. - 2 \frac{H_{i,j}^3}{R_{i,j} \bar{\mu}_{i,j} \beta^2 \Delta \bar{\theta}^2} - \frac{H_{i,j+1}^3}{R_{i,j} \bar{\mu}_{i,j+1} \beta^2 \Delta \bar{\theta}^2} - \frac{H_{i,j-1}^3}{R_{i,j} \bar{\mu}_{i,j-1} \beta^2 \Delta \bar{\theta}^2} \right] \\
 & = \frac{6R_{i,j}}{\Delta \theta} [H_{i,j+1} - H_{i,j-1}] + 12R_{i,j} \beta V \quad (5)
 \end{aligned}$$

The calculation procedure uses these calculated pressures along with numerical methods for integration to obtain the load capacity, radial and angular location of centre of pressure. To ensure numerical accuracy the pressure distribution satisfied the 0.1 percent convergence limit.

4. DYNAMIC COEFFICIENTS

a) The damping of the fluid film is its ability to absorb energy and is measured in N.sec/m. The damping coefficient, C_z , was calculated using

$$C_z = \frac{\Delta W}{\Delta V} \quad (6)$$

The subscript 'z' refers to the vertical direction of motion, orthogonal to the direction of the applied forces. Where W is the component of force causing displacement, measured in N, and V is the vertical velocity, measured in m/s. The formula for calculation of non-dimensional damping coefficient as in [6] is

$$C_z^* = C_z \frac{U}{L} \left[\frac{h_{\min}^3}{BL^2 U \mu_{eff}} \right] \quad (7)$$

b) Similarly the stiffness of the fluid film is its ability to resist deformation by an applied force measured in N/m. The stiffness coefficient, K_z was calculated using

$$K_z = \frac{\Delta W}{\Delta h_o} \quad (8)$$

The formula for calculation of non-dimensional stiffness coefficient

$$K_z^* = K_z \left[\frac{h_{\min}^3}{BL^2 U \mu_{eff}} \right] \quad (9)$$

5. CALCULATION OF DYNAMIC COEFFICIENTS

Spring arrangement of pad is shown in figure 3. The non-dimensional damping and stiffness characteristics are calculated for 1) Authors' data and 2) Yuan's data (Case 1) as in [7] as listed in table 1. Initially substituting the values of a and h_0 in the equation of the shape of the oil film we gradient film thickness coefficients.

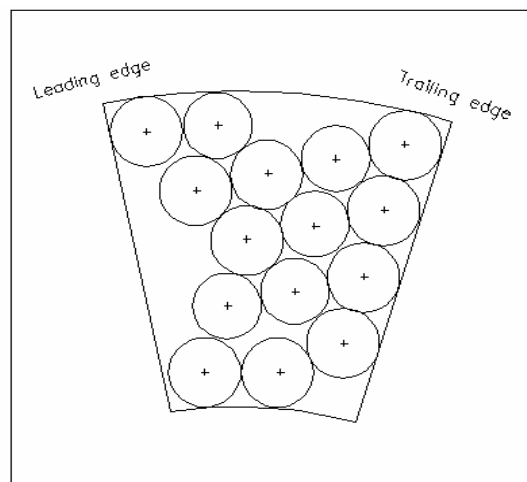


Figure 3. Spring arrangement of pad

Table 1. Thrust Bearing Geometry

	Yuan's data (Case 1)	Author's data
Outer Diameter (m)	1.168	1.275
Inner Diameter(m)	0.711	0.75
Number of Pads	12	6
Thickness (mm)	41.1	--
Groove width(mm)	52.3	84
Number of Springs	15	-
Operating Conditions		
Load (MN)	2.124	--
Rotational speed (rads/s)	52.4	14.28
Oil pot temperature (° C)	70	40
Oil properties		
ISO grade	46	--
γ (cSt) at 40 ° C	48	73
γ (cSt) at 100 ° C	6.70	10.7
ρ (g/m) at 15 ° C	0.873	0.861

6. RESULTS AND DISCUSSIONS

By substituting these values of gradient film thickness in modified Reynolds' equation we get pressure at each node. Figure 4 shows 3-D pressure distribution in the oil film of a flat pad. By numerical integration to these pressure points we get the load .The values of W and V are varied from +10% to -10% and the difference of these values are taken ie. ΔW and ΔV . Table 2 shows damping coefficients calculated for the author's parameters.

Table 2. Values of ' C_z ' Corresponding to ' ΔW ' and ' ΔV '

	$\pm 2\%$	$\pm 4\%$	$\pm 6\%$	$\pm 8\%$	$\pm 10\%$
ΔW	263.8	425.6	796.6	1068.2	1616.7
ΔV	.293e-4	.594e-4	.89e-4	1.49e-4	1.49e-4
C_z	888e4	716e4	894e4	717e4	1088e4
C_z^*	$1.4 \cdot 10^{-8}$	$3.0 \cdot 10^{-8}$	$3.7 \cdot 10^{-8}$	$3.0 \cdot 10^{-8}$	$4.5 \cdot 10^{-8}$

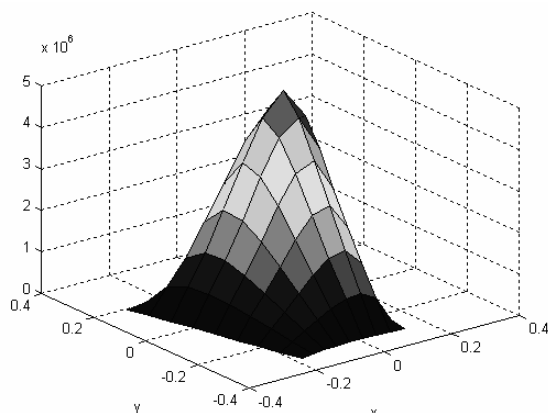


Figure 4. 3-D pressure distribution in the oil film of a flat pad, $a=1.8$

For the values of 'a' taken from 1.0 to 2.2 and L/B ratio from 0.7 to 1.3 the damping values are calculated. A contour plot depicting the damping values at 'a' and 'L/B' respectively is drawn as shown in figure 5.

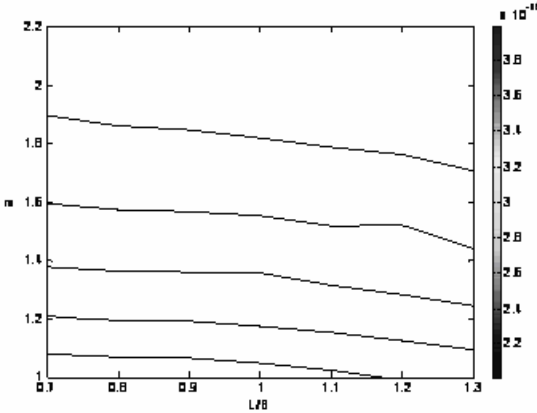


Figure 5. Non-Dimensional Damping C_z with respect to a and L/B ratio

The values of W and h_0 are varied from 10% to -10% and the difference of these values are taken as ΔW and Δh_0 . Table 3 shows calculated values of ' K_z '

Table 3. Values of ' K_z ' corresponding to ' ΔW ' and ' Δh_0 '

	$\pm 2\%$	$\pm 4\%$	$\pm 6\%$	$\pm 8\%$	$\pm 10\%$
ΔW	263.8	425.6	796.6	1068.2	1616.7
Δh_0	.0052	.0104	.0156	.0208	.0260
K_z	50678	40880	51011	51302	62116
K_z^*	$5.0 \cdot 10^{-9}$	$4.0 \cdot 10^{-9}$	$5.0 \cdot 10^{-9}$	$5.0 \cdot 10^{-9}$	$6.1 \cdot 10^{-9}$

Similarly sample Stiffness values for L/B ratio 0.7 to 1.3 for 'a' taken from 1.0 to 2.2 are calculated. Based on these values a contour plot as shown in figure 6, is drawn between 'a' and 'L/B' ratio. The contours in the graph represent the stiffness values at 'a' and 'L/B' respectively. The colour bar represents the value of stiffness at respective 'a' and 'L/B' values.

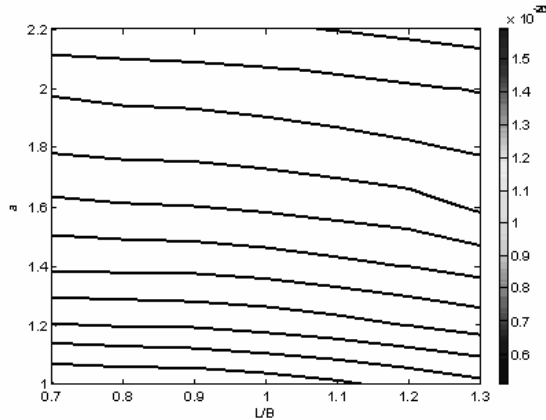


Figure 6. Non-Dimensional Stiffness K_z with respect to a and L/B Ratio

The corresponding non-dimensional damping and stiffness values for **Yuan's parameters**, are listed in tables 4 and 5.

Table 4: Yuans' values of ' C_z^* ' corresponding to ' ΔW ' and ' ΔV '

	$\pm 2\%$	$\pm 4\%$	$\pm 6\%$	$\pm 8\%$	$\pm 10\%$
ΔW	20.67	41.42	62.39	83.65	105.31
ΔV	.00034	.00068	.001011	.00135	.0051
C_z	61325	61454	61711	62055	60788
C_z^*	$6.6 \cdot 10^{-9}$	$6.6 \cdot 10^{-9}$	$6.6 \cdot 10^{-9}$	$6.7 \cdot 10^{-9}$	$6.2 \cdot 10^{-9}$

Table 5: Yuans' values of ' K_z^* ' corresponding to ' ΔW ' and ' Δh_o '

	$\pm 2\%$	$\pm 4\%$	$\pm 6\%$	$\pm 8\%$	$\pm 10\%$
ΔW	20.67	41.42	62.39	83.65	105.31
Δh_o	$2.7 \cdot 10^{-7}$	$5.3 \cdot 10^{-7}$	$8 \cdot 10^{-7}$	$1.1 \cdot 10^{-6}$	$1.3 \cdot 10^{-6}$
K_z	77,706767	77,857143	78,57,6826	78,915094	79180451
K_z^*	$2.0 \cdot 10^{-8}$	$2.1 \cdot 10^{-8}$	$5.7 \cdot 10^{-9}$	$5.6 \cdot 10^{-9}$	$5.7 \cdot 10^{-9}$

As done for the author's dimensional parameters non-dimensional damping and stiffness values are calculated for 'a' taken from 1.0 to 2.2 and L/B ratio from 0.7 to 1.3. Based on these damping coefficient values a contour plot viz. figure 7, is made. Figure 8 shows a contour plot representing the stiffness values at 'a' and 'L/B' respectively.

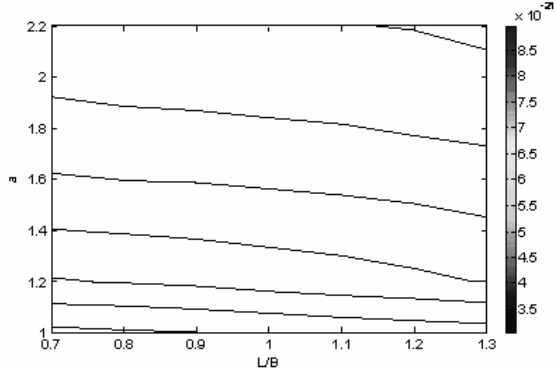


Figure 7. Yuan's non-dimensional damping C_z with respect to a and L/B ratio

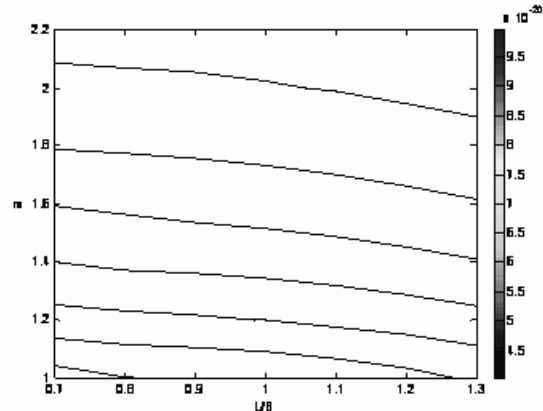


Figure 8. Yuan's non-dimensional stiffness K_z with respect to a and L/B ratio

For the authors' non-dimensional values the damping coefficient value at $L/B = 0.7$ and $a=1$ is $4.3114e-18$ and it decreases gradually as 'a' and L/B are increased and finally at $a = 2.2$ and $L/B = 1.3$ the value of non-dimensional damping coefficient becomes $1.5006e-18$. The value of the non-dimensional stiffness coefficient at $L/B = 0.7$ and ' a ' = 1.0 is $1.6006e-20$ and it increases gradually and at ' a '= 2.2 and $L/B = 1.3$ is equal to $4.5713e-21$. For Yuans' non dimensional values the corresponding maximum damping coefficient value is $9.2386e-21$ and it decreases gradually to a minimum of $2.8014e-21$.The corresponding non-dimensional minimum value of the stiffness coefficient is $1.0421e-19$ and it increases gradually to $3.2175e-20$.

7. CONCLUSION

Two dimensional Reynolds' equation is modified and a finite difference method based solution procedure for finding pressure values is written and verified. Numerical integration to these pressure points gives the load. Good agreement occurred between the theoretical and experimental film thicknesses. Non-dimensional damping and stiffness coefficients for the variation of film thickness and introduction of vertical velocity were determined. The variation pattern for the damping and stiffness coefficient values for the two sets of dimensions under consideration is similar. The Non-dimensional numerical values for the two cases are comparable and marginally vary such that both damping and stiffness coefficient values are greater for the author's dimensions. This proves the fidelity of our software package to analyse dynamic characteristics of large diameter thrust bearings.

NOMENCLATURE

- a: it is the between ratio of the difference inlet film thickness and outlet film thickness to the outlet film thickness
- b: length of the bearing, m U, V: velocity along and normal to surface, m/s
- W: load on bearing, N
- G_P: gap between the pads, m
- h_o: oil film thickness at the trailing edge, m
- m: number of the nodes on the grid in radial direction
- n: number of the nodes in circumferential direction coordinate along n -axis.
- p: pressure in the oil film , Pa

r: radial coordinate
 Δr : division on the grid along radial direction,
 r: radius of the runner, m
 t: transit time, B/U, s
 B: circumferential length of the thrust segment, m
 C_z : bearing damping coefficient, N-s/m
 C_z^* : non-dimensional damping coefficient
 D_i : inner diameter of the thrust bearing, m
 D_o : outer diameter of the thrust bearing, m
 F0, F2, F3: viscosity integrals in the Reynolds' equation
 H: non-dimensional thickness of the oil film, h/h0
 K_z : bearing stiffness coefficient, N/m
 K_z^* : non-dimensional stiffness coefficient
 L : radial length of the thrust pad, m
 N : angular speed of the runner, rpm
 P: non-dimensional pressure
 P: pressure matrix in Reynolds' equation
 R: non-dimensional radius , r/r_0
 Z: no. of pads
 γ : film thickness ratio
 μ : viscosity of oil , Pa.s
 θ: angle from the leading edge, rad
 ρ : density of oil, kg/m3
 ω : angular speed of the runner, rad/s
 $\Delta\theta$: angular division of the grid,rad
 i: index of the node in radial direction
 j: index of the node in circumferential direction

REFERENCES

- [1] C.F. Kettleborough, *On the Transient Response of the Thrust Bearing*, in: *Proceedings of ETCE2002, ASME Engineering Technology Conference on Energy*, February 4-5, 2002. Houston, TX., pp 1029-1040.
- [2] Q. Zhu, W.J. Zhang: *A preliminary non linear analysis of the axial transient response of the sector shaped hydrodynamic thrust bearing rotor system*, Transactions of ASME- Journal of Tribology, Vol.125, October, pp.854-858. 2003
- [3] C.M.M. Ettles, and H.G Anderson, *Three – Dimensional Thermo – Elastic solutions of thrust bearings using code Marmac 1*, Transactions of the ASME-Journal of Tribology, Vol.112, pp.405-412. 1991
- [4] K.K. Chaturvedi, K. Athre, Y. Nath, and S.Biswas:, *Refinement in Estimation of Load Capacity and Temperature Distribution of Pad Bearing*, *Proceedings of Eurotrib-89*, June 1989 Helsinki, Finland.,
- [5] J.W. Capitao, *Influence of Turbulence on Performance characteristics of the TiltingPad Thrust Bearing*, Transactions of the ASME- Journal of Lubrication Technology, January, pp.110-117.1974
- [6] Eskild Storteig, Maurice F. White, *Dynamic Characteristics of hydrodynamically lubricated fixed-pad thrust bearings*, Wear, Vol.232, pp.250-255, 1999
- [7] J.H. Yuan., J.H Ferguson and J.B Medley. *Spring Supported Thrust Bearings Hydroelectric Generators: Comparison of Experimental Data with Numerical Predictions*, *Tribology Transactions*. Vol.44, pp. 27-34., 2001.